Heritage Science

A multi-analytical study of the palette of impressionist and post-impressionist Puerto Rican artists

Marc Vermeulen[1], Annette S. Ortiz Miranda[1,4], Diego Tamburini[2], Sol E. Rivera Delgado[3] and Marc Walton[1,5*]

Abstract

This paper presents the pigment characterization in six impressionist and post-impressionist paintings by three leading Puerto Rican artists: Francisco Oller (1833–1917), José Cuchí y Arnau (1857–1925), and Ramón Frade (1875–1954). The paintings, belonging to the Corporación de las Artes Musicales and Museo de Arte de Puerto Rico (San Juan, Puerto Rico), were investigated through a combination of complementary non- and micro-invasive scientific techniques. The use of non-invasive macro-X-ray fluorescence (MA-XRF) and reflectance imaging spectroscopy (RIS) was applied for the first time to characterize Puerto Rican artists' palette. The non-invasive approach was integrated with spectroscopic techniques such as Raman and/or Fourier-transform infrared (FTIR) spectroscopy, as well as high pressure liquid chromatography coupled to diode array detector and tandem mass spectrometry (HPLC-DAD-MS/MS), when sampling was possible. While this technical investigation reveals pigments that are typical for late 19th/early twentieth century paintings, it also emphasizes some unexpected findings, including the use of cobalt green and synthetic yellow lakes, which enabled the date given to some of the paintings to be refined to post 1910 rather than their current dates of ca. 1890. This study confirms that the Puerto Rican artist's palettes are very similar to their European contemporaries, underscoring both their European training and their attempt to adapt these methods of painting to a new Caribbean identity emerging from the Spanish American War.

Keywords: Caribbean art, MA-XRF, Reflectance imaging spectroscopy, HPLC-DAD-MS/MS, Synthetic organic pigments, Francisco Oller

Introduction

When one thinks of impressionist and post-impressionist painters (Monet, Renoir, Pissarro, and Cezanne, to only cite a few), Puerto Rican artists may not be the first that come to mind. However, Puerto Rico—a Spanish colony until 1898—produced several late-19th/early twentieth century masters, including Francisco Oller (1833–1917) who became known as the first Latin American painter to adopt the impressionists' artistic vocabulary of light and color to document the Puerto Rican landscape. His

paintings of sugarcane plantations and still-lives of tropical fruits are eagerly sought by private collectors and found in many major museums around the world, including the Musée d'Orsay, the Brooklyn Museum, the Museo del Barrio, and several cultural institutions in Puerto Rico (Museo de Arte de Ponce, Instituto de Cultura Puertorriqueña and Corporación de las Artes Musicales on indefinite loan at the Museo de Arte de Puerto Rico) [1]. While he had initial art training in San Juan, he went abroad for further study in Spain and France, where he painted with Monet and even introduced Camille Pissarro, another Caribbean native from the Danish West Indies, to Paul Cézanne [1]. Unlike Pissarro, however, Oller chose not to stay in Europe and instead settled in Puerto Rico where he remained until his death in 1917.

*Correspondence: marc.walton@mplus.org.hk
[1] Northwestern University, Art Institute of Chicago Center for Scientific Studies in the Arts (NU-ACCESS), 2145 Sheridan Road, Evanston, IL 60208, USA
Full list of author information is available at the end of the article

Vermeulen *et al. Heritage Science*   (2022) 10:44

Page 2 of 22

Oller's artistic influence was significant and today he is recognized as one of the foremost artists to express a Caribbean visual culture and identity [1].

Oller's work depicting Puerto Rico also influenced many other Puerto Rican artists, such as José Cuchí y Arnau (1857–1925) and Ramón Frade (1875–1954). Many from this next generation of Puerto Rican artists followed in Oller's footsteps and left the island to be trained abroad. Notably, in 1874, José Cuchí y Arnau moved to Barcelona where he was known for his portraits representing popular characters of Spanish culture [2]. In contrast, Ramón Frade was trained in the Dominican Republic under the supervision of Spanish and French teachers, later becoming a major champion for producing artistic works that helped establish a Puerto Rican identity [3]. Further emphasizing their embrace of the European culture, Cuchí y Arnau was awarded a gold medal at the Paris Exposition Universelle in 1900 while Frade exhibited his works at the Paris Salon that same year.

Through their ties with Puerto Rico and the Caribbean in general, these artists helped transform painting in the Caribbean through a vibrant exchange of ideas, materials, and the latest technical developments in early European paintings. In the early 1900, European artistry started shifting toward more avant garde movements such as fauvism, expressionism, and cubism [4, 5]. Yet, these Puerto Rican artists chose to hold on to a more representational style to appeal to a Caribbean-centered audience. While the color palette and technique of French and American impressionist and post-impressionist artists have been extensively studied [6–11], Puerto Rican artists have not attained the same level of appreciation as their European contemporaries, reached the same broad audiences, nor received the same scientific attention. Consequently, little is known about their use of materials and painting techniques.

To redress this gap in our knowledge about the painting methods of the 'Caribbean impressionists,' this investigation considers six paintings by Francisco Oller, José Cuchí y Arnau and Ramón Frade. Primarily MA-XRF and reflectance imaging spectroscopy (RIS) are used here to identify pigments and map their distribution in paintings based on the pigments' specific elemental composition and molecular response [12–16]. For example, vermilion (HgS), which is the only (red) artist pigment containing Hg, and for which the reflectance spectrum has a specific inflection point around 590 nm, is easily identified through its elemental and molecular characterization [17]. On the other hand, pigments such as Emerald and/or Scheele's greens have a very specific elemental composition (Cu and As) as determined by their XRF responses, yet can have a reflectance spectrum similar to a mixture of Prussian blue and a yellow pigment such as chrome
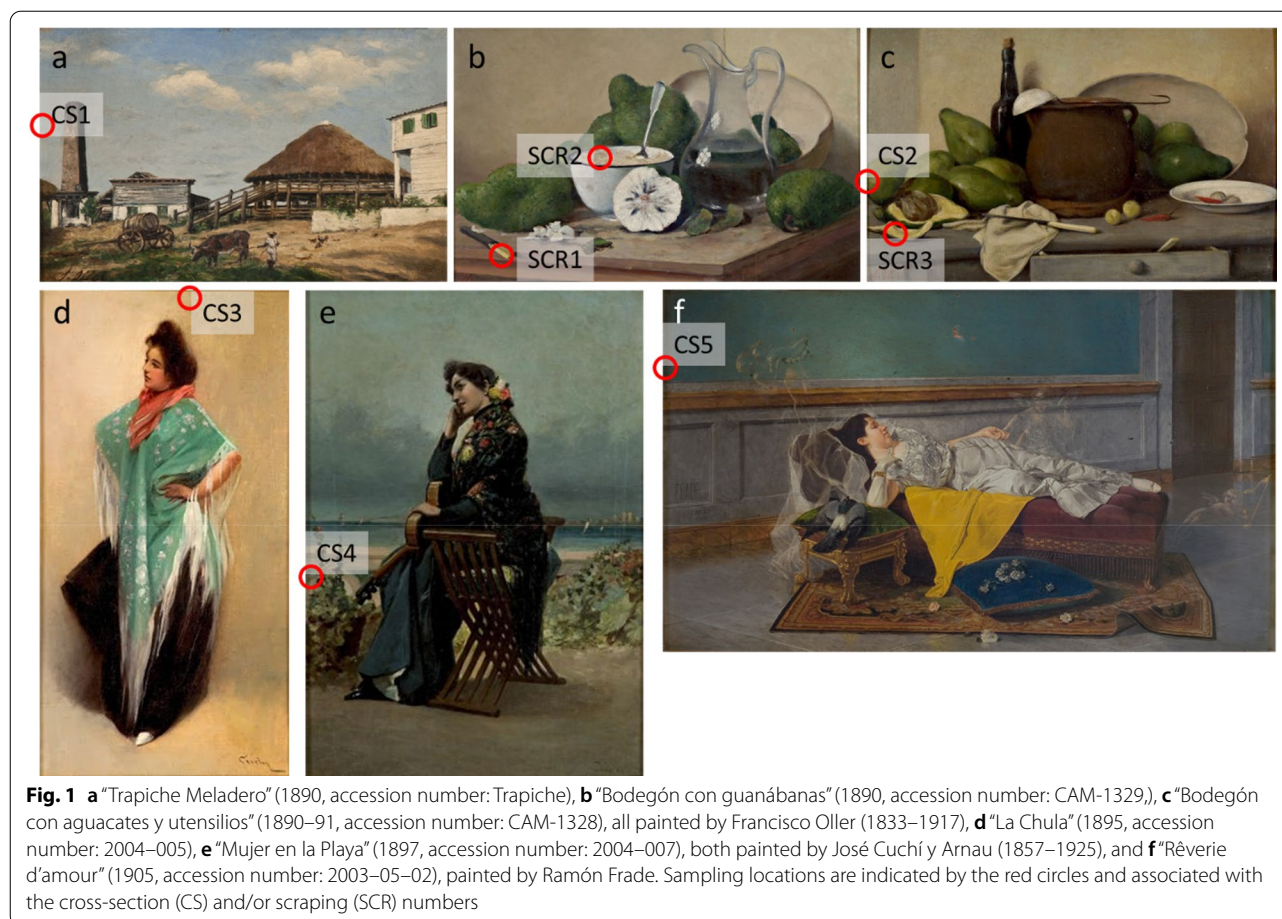
yellow [18, 19]. While usually not identified solely by MA-XRF [20], Prussian blue and ultramarine blue have unique reflectance spectra, which allow for their unambiguous identification. Apart from yellow ochres, which have a very specific reflectance spectrum [17], yellow colorants, in general, are difficult to identify through RIS. However, MA-XRF is often considered specific enough that it becomes possible to associate elemental co-presence with a specific yellow pigment, e.g., Pb/Sn being a strong indication for lead tin yellow; Pb/Cr pointing towards chrome yellow; Pb/Sb for Naples yellow; Ba/Cr indicative of lemon yellow, etc. Therefore, as shown by our examples here, by coupling both techniques, it becomes easier to differentiate between various pigments or mixtures of pigments for a given color, based on the combination of the color analyzed, its elemental composition and reflectance spectrum. Nevertheless, while very informative about the spatial distribution of tentatively identified pigments, MA-XRF only provides elemental composition and the electronic transitions associated with RIS typically produce a broad and sometimes unspecific molecular response which means that the association of additional complementary spectroscopic methods are sometimes needed for an unambiguous pigment identification. For this study we also employed Raman as well as scanning electron microscopy coupled to energy dispersive X-ray spectrometry (SEM-EDX) [16, 21] on embedded paint micro-samples to better characterize the nature of the pigments used. In the case of organic colorants, chromatographic techniques, such as high pressure liquid chromatography (HPLC) coupled to diode array detector (DAD) and/or mass spectrometry (MS) applied to micro-samples were integrated into the analytical protocol [22].

Following this rationale, this study represents an opportunity to investigate the material influence of various cultures (European, American, and Caribbean) on the late nineteenth century artistic production in Latin America through the identification of the artists' palette. While scholarship on the philosophical and art historical perspectives of Latin American and Caribbean artists from the nineteenth century is already robust [23–31], no studies have been conducted to address materials comprising the Puerto Rican artistic palette. This study sets a foundation for further studies focusing on Caribbean and Central American art.

Materials and methods
Paintings
Figure 1 presents the six paintings by Puerto Rican artists belonging to Corporación de las Artes Musicales and the permanent collection of the Museo de Arte de Puerto Rico (San Juan, Puerto Rico) that were analyzed during

Fig. 1 **a** "Trapiche Meladero" (1890, accession number: Trapiche), **b** "Bodegón con guanábanas" (1890, accession number: CAM-1329,), **c** "Bodegón con aguacates y utensilios" (1890–91, accession number: CAM-1328), all painted by Francisco Oller (1833–1917), **d** "La Chula" (1895, accession number: 2004–005), **e** "Mujer en la Playa" (1897, accession number: 2004–007), both painted by José Cuchí y Arnau (1857–1925), and **f** "Rêverie d'amour" (1905, accession number: 2003–05–02), painted by Ramón Frade. Sampling locations are indicated by the red circles and associated with the cross-section (CS) and/or scraping (SCR) numbers

this study. According to biographical and historical data, all six paintings were likely to have been made between 1890 and 1905: a time of important political and social changes in Puerto Rico. Table 1 summarizes all information associated with the six paintings studied.

When possible, paint microsamples were removed with a scalpel from selected locations of the paintings, mostly on the edges, to investigate the ground composition, the layer build-up and some of the pigments used. The localization of the various samples is indicated by the red circles in Fig. 1.

Some samples were mounted as cross-sections (CS1–5) prior to analysis. The cross-sections were prepared by embedding the specimens in Buehler Epo Thin 2 epoxy. The cured cross-sections were polished under a flow of water with Buehler polishing cloths with a sequence of grits from 500 to 2400 grade until the fragment surface was nearly exposed. Dry polishing was continued using a 1 µm diamond suspension (Buehler MetaDi) to expose the samples and obtain a mirror-like surface. The paint cross-sections were rinsed in hexane to reduce resin contaminations.

MA-XRF

The MA-XRF scanner developed at NU-ACCESS [32] was used to scan the entire surface of all six paintings. The instrument is equipped with a transmission 12 W Rh anode X-Ray tube (MOXTEK Inc., Orem, UT) coupled to a removable polycapillary optic (XOS Inc., East Greenbush, NY) yielding a beam diameter of 100 µm at a 4.8 cm focal point. Two laser pointers, mounted in such a way that their intersection point coincides with the cross-point of the incident X-ray beam and detector axis, allow for optimizing both excitation and detection conditions. X-rays are detected by means of a 50 mm^2 active collimated area Silicon Drift Detector (SDD, Bruker Nano Analytics), equipped with a CUBE preamplifier associated with DANTE digital pulse processor (DANTE DPP, Bruker Nano Analytics), with an energy resolution of 132 eV at the Mn Kα line (5.9 keV). The instrument was operated at 30 kV and 400 µA. The elemental 2D mapping of the objects surface was achieved through an automatic XY raster scanning with varying per pixel acquisition times and step size. The detailed per pixel acquisition times and step size used for each painting

Table 1 Summary of the analyzed paintings

Painting's original titles	Artist	Year of creation	Dimension	Medium	Object number	Painting thumbnail	Cross section/ samples
Trapiche meladero	Francisco Oller	1890	43.8 × 52.1 cm	Oil on canvas	Trapiche		CS1
Bodegón con guaná-banas		Circa 1890	52.1 × 80 cm	Oil on wood	CAM-1329		SCR1 SCR2
Bodegón con agua-cates y utensilios		1890–91	52.4 × 83.8 cm	Oil on canvas	CAM-1328		CS2 SCR3
La Chula	José Cuchí y Arnau	1895	68.6 × 109.2 cm	Oil on canvas	2004–005		CS3
Mujer en la playa		1897	49.5 × 34.9 cm	Oil on canvas	2004–007		CS4
Rêverie d'amour	Ramón Frade	1905	35.9 × 61 cm	Oil on wood	2003–05–02		CS5

are given in Additional file 1: Table S1. The elemental maps were produced using PyMCA software [33]. In the case when several maps were required to scan the entire painting, the various maps were stitched together using registration and stitching plugins available in the open-source image processing package Fiji suite [34, 35].

Reflectance imaging spectroscopy (RIS)

RIS data were acquired using a Resonon Pika II Pushbroom system (Resonon, Inc., Bozeman, MT, USA) in the 400–900 nm range with spectral resolution of 2.1 nm, with a total of 240 channels. The system was connected to a stage allowing the scanning of about 30 cm of the object's width, with an integration time of 1 s, and a spatial per-pixel resolution of 0.3×0.3 mm or 0.5×0.5 mm depending on the distance between the painting and the camera's objective (which was changed according to the paintings dimensions to accommodate the access time to the paintings). The spatial resolution and varying number of cubes acquired for each painting are indicated in Additional file 1: Table S1. During acquisition, the object was illuminated using two broad spectrum tungsten halogen lamps placed at 45° of the objects normal. A Spectralon diffuse white reflectance standard (Labsphere, North Sutton, USA) was used as a calibration target to convert the image cubes to diffuse reflectance. Hyperspectral acquisition was performed using the SpectrononPro software (Resonon, Inc., Bozeman, MT, USA). The raw hyperspectral data cubes were converted to a tiff stack in Fiji and the partially overlapping areas of two cubes from the same painting were registered and stitched together using the open-source image processing package Fiji suite [34, 35], prior to further processing. The final complete cube and its RGB image were registered to MA-XRF maps for comparison purposes.

Spectral stacks were further processed using our previously described software pipeline [36] that utilizes UMAP, density cluster mapping, and non-negative least square fitting procedure to extract the various pigments spectra (endmembers) and recreate their distribution

Vermeulen *et al. Heritage Science*   (2022) 10:44

Page 5 of 22

maps. The data processing was performed in a Jupyter Notebook running in Python. The cosine distance metric was used for the data reduction and a number of neighbors of 10 was chosen by default for the density clustering as described by our protocol [36]. The threshold and minimum distance used for the 2d histogram were tailored to each painting and are given in the associated figure legends.

Comparison of the reflectance spectra with the in-house, published, and online databases [17, 22, 37, 38] was used to tentatively identify the pigments employed. Pigment possibilities were also narrowed down with the help of the elemental distribution maps obtained using MA-XRF.

SEM–EDX

Backscattered electron (BSE) images and elemental distribution maps of cross-sections were acquired with a Hitachi S-3400N-II SEM (Hitachi, Tokyo, Japan) equipped with a INCAx-act EDS detection system (Oxford Instruments, Abingdon, United Kingdom) all operated under variable pressure vacuum (60 Pa). Images and elemental maps were recorded using an acceleration voltage of 20 kV and a 90-mA probe current. EDS analyses were performed with a working distance of 10 mm and a minimum of 300,000 counts/spectrum. Data was collected and processed using the AZtec software system, v. 3.3 (Oxford Instruments, Abingdon, United Kingdom).

Raman spectroscopy

Spectra were acquired with a HORIBA LabRAM HR Evolution Confocal Raman spectrometer equipped with an Olympus $50 \times$ long working distance objective and a charge-coupled device (CCD) detector. A continuous wave diode laser (Laser Quantum) and a solid-state laser (Horiba Scientific), emitting light at 532 and 785 nm respectively, were used as the excitation sources and a 600 ruling/mm holographic grating provided a spectral resolution of 3.2 cm^{-1}. The output laser power was kept below 25 mW, while the number of scans and integration time were adjusted to prevent damage from overheating and according to the spectral response of the samples examined. All spectra were acquired using the HORIBA LabSpec 6 Spectroscopy Suite Software. Pigments identification was undertaken using previously published spectra and online databases [39, 40].

HPLC–DAD-ESI-Q-ToF

Two micro-samples (approximately 50 µg) taken from CAM-1328 and CAM-1329 (SCR3 and SCR2 respectively) were analyzed by high pressure liquid chromatography coupled to diode array detector and electrospray ionization followed by quadrupole and time of flight detection (HPLC-DAD-ESI-Q-ToF). The molecular extraction was performed using a method published in [22], which briefly consists of a double mild extraction procedure, using DMSO first, and secondly a mixture of methanol/acetone/water/0.5 M oxalic acid 30:30:40:1 (v/v/v/v).

Analyses were carried out using a 1260 Infinity HPLC (Agilent Technologies), coupled to a 1100 DAD detector (Hewlett-Packard) and to a Quadrupole-Time of Flight tandem mass spectrometer 6530 Infinity Q-ToF detector (Agilent Technologies) by a Jet Stream ESI interface (Agilent Technologies). Separation was achieved using a Zorbax Extend-C18 column (2.1 × 50 mm, 1.8 µm particle size) with a 0.4 mL/min flow rate and 40 °C column temperature, and a gradient of water with 0.1% formic acid (eluent A) and acetonitrile with 0.1% formic acid (eluent B). The elution gradient was programmed as follows: initial conditions 95% A, followed by a linear gradient to 100% B in 10 min, and held for 2 min. Re-equilibration time for each analysis was 10 min. Ten µL injection volume was adopted for MS experiments and 20 µL for MS/MS experiments.

The DAD detector (cell volume 50 µL) scanned in the range 190–700 nm with 2 nm resolution. The ESI operating conditions were: drying gas (N$_2$, purity > 98%) temperature 350 °C and 10 L/min flow; capillary voltage 4.0 kV; nebulizer gas pressure 40 psig; sheath gas (N$_2$, purity > 98%) temperature 375 °C and flow 11 L/min. High resolution MS and MS/MS spectra were acquired in both negative and positive mode in the range 100–1700 m/*z*. The fragmentor was kept at 100 V, nozzle voltage 1000 V, skimmer 65 V, octapole RF 750 V. For the MS/MS experiments, different voltages (from 10 to 40 V) in the collision cell were tested for Collision Induced Dissociation (CID), in order to maximize the information obtained from the fragmentation of the single molecules. The collision gas was N$_2$ (purity 99.999%). The data were collected by targeted MS/MS acquisition with an MS scan rate of 1.0 spectra/sec and a MS/MS scan rate of 1.0 spectra/sec. Auto-calibration was performed daily using Agilent tuning mix HP0321 (Agilent Technologies) prepared in 90% water-10% acetonitrile.

MassHunter Workstation Software was used to carry out diode array detector and mass spectrometer control, data acquisition, and data analysis. In particular, extract ion chromatograms were obtained using the software EIC function and selecting the mass range corresponding to the calculated mass ± 0.01 m/*z*.

Results

Non-invasive imaging techniques: MA-XRF and RIS

The color scheme of the paintings studied is rather simple and incorporates mostly shades of white, blue, green, red,

yellow, and brown. The MA-XRF distribution maps, RIS endmember maps and associated reflectance curves for CAM-1329 are presented in Figs. 2 and 3, respectively. A similar train of thought was followed for the distribution maps (MA-XRF and RIS) of the five other paintings by Oller, Cuchí y Arnau and Frade. The corresponding results are shown in Supplementary Information (Additional file 1: Figs. S1–S10) and a summary of the results and tentative pigment identifications obtained from the non-invasive imaging techniques are reported in Table 2 for all paintings under investigation.

The XRF maps of Pb suggest a lead-based ground, likely to be lead white (lead carbonate and/or basic lead carbonate), due to Pb being found throughout the compositions. Further indications of the presence of Pb in the lower layers are given by the shielding effect of overlying heavy elements, such as Co, Zn, Cr, and Cu, which serve to block the Pb signal found underneath. The lack of Pb in small areas of loss where Ca, Fe, Ti, Ba, Ti, and K—most likely used during previous conservation treatments—are found, also indicates that Pb was used in the ground layer. The large ochre-based conservation intervention in the area of loss in the plate is further confirmed using RIS (Fig. 3-EM1).

The presence of Hg in the redder areas such as the brown of the table or the edges of the plate (Fig. 2-Hg), the red peppers in CAM-1328 (Additional file 1: Fig. S3-Hg), and the red scarf in 2004–005 suggests the use of vermilion (mercury sulfide): the sole pigment containing mercury. The use of vermilion is further suggested by RIS, with the characteristic inflection point at 585–590 nm (Fig. 3-EM6, Additional file 1: Fig. S4-EM7, Fig. S10-EM5). However, the complex curves observed with absorbances at 455, 560, and ca. 640 nm (Fig. 3-EM6, Additional file 1: Fig. S6-EM6, Fig. S10-EM5) may also suggest the use of an oxide/oxy-hydroxide-based ochre mixed with vermilion.

XRF maps also imply the presence of a Cr-based green in most green areas of the composition, including the guanábanas (Fig. 2-Cr). The Cr-based pigment is likely to be viridian (hydrated chromium oxide), chrome(III)oxide green and/or a mixture of chrome yellow and blue pigments. The spectral features, and specifically the shoulder at 705 nm observed in RIS (Fig. 3-EM3–5), tend to
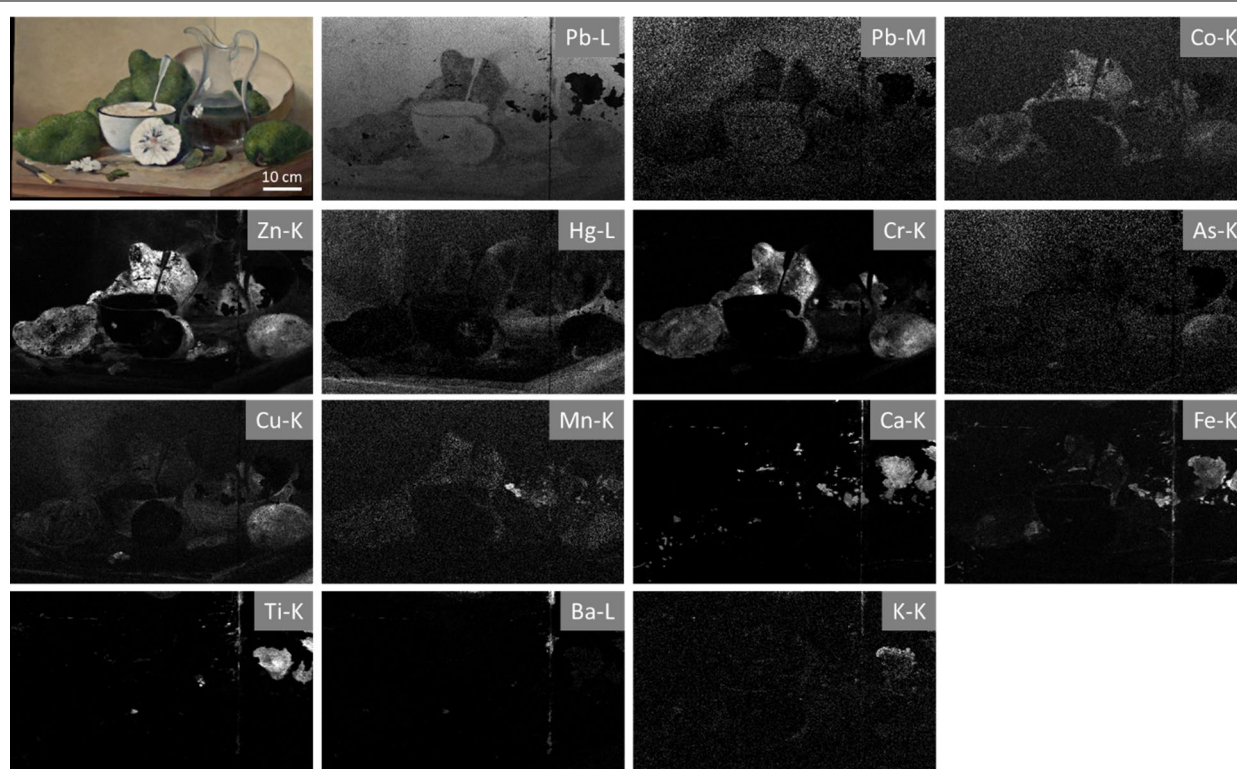
Fig. 2 Registered RGB and MA-XRF elemental maps obtained for CAM-1329. Elemental maps for Ca, Fe, Ti, Ba and K appear to be associated with conservation intervention whereas Pb, Co, Zn, Hg, Cr, As, Cu, Mn and some Fe appear associated with the original paint layer. Elemental distribution maps suggest the use of a lead-based ground (likely to be lead white); ochre-based retouching (Ti, K, Fe, Ca, K); cobalt blue/zinc white and/or cobalt green pigment (Co/Zn); pigment mixtures containing chrome-based green (Cr); vermilion (Hg); Emerald/Scheele's green (Cu/As); and possibly umber pigment (Fe/Mn)

Fig. 3 Registered RGB, RIS distribution maps and associated reflectance curves for each identified endmember (EM) in CAM-1329. RIS distribution maps suggest the use of an ochre-based retouching (EM1); ultramarine blue (EM2); green pigment mixtures containing ultramarine blue (EM3, EM4 and EM5); vermilion and ochre mixture (EM6); a possibly Emerald/Scheele's green pigment (EM7); and unknown yellow pigments (EM8 and EM9). Sharp bands at 437, 543, and 610 nm (marked with an asterisk) are associated with light pollution from nearby ambient lightning. Threshold and minimum distance values of respectively 0.1 and 15 were used for the RIS endmembers extraction procedure

indicate the use of viridian or chrome(III)oxide green, rather than a mixture of chrome yellow and blue pigments; however, neither MA-XRF nor RIS allows for their differentiation, hence Raman spectroscopy was applied (section "Micro-invasive investigation: optical microscopy, SEM–EDX, and Raman spectroscopy"). The use of viridian and/or chrome(III) oxide green is also implied in the grass and binds of Trapiche Meladero and in the dress of the woman in 2004.005 based on the presence of Cr in MA-XRF (Additional file 1: Fig. S1-Cr and Fig. S5-Cr) and RIS spectra features similar to what is observed in CAM-1329, namely the increased absorbance at 450 and 600 nm and the shoulder at 705–710 nm (Additional file 1: Fig. S2-EM2 and Fig. S6-EM7). Conversely, a mixture of chrome yellow and a blue pigment (likely to be

Prussian blue based on the lack of elemental response and the RIS data, Additional file 1: Fig. S10-EM4) is identified in the green seat cover in 2003–05–02.

The Cr-based green does not appear to be the sole green pigment used in CAM-1329. The co-occurrence of As and Cu also suggests that Oller used Emerald green (copper acetoarsenite) and/or Scheele's green (copper arsenite, Fig. 2-As/Cu) in the green highlights of the fruits. Such co-occurrence was also observed in the avocados in CAM-1328 (Additional file 1: Fig. S4-As/Cu) and in the dark colored shawl of the woman seating by the sea in 2004–007 (Additional file 1: Fig. S7-As/Cu). The presence of the emerald and/or Scheele's green was also confirmed by RIS through the inflection point and maximum absorbance at 505 and 670 nm, respectively

Vermeulen *et al. Heritage Science*　(2022) 10:44

Page 8 of 22

Table 2 Overview of the materials identified or tentatively identified through non-invasive analysis of the six paintings investigated

Painting	Color	MA-XRF/SEM-EDX			Reflectance spectroscopy/µ-reflectance spectroscopy			
		Element	Figure/ distribution map	Tentative pigment identification	Distribution map/spectrum	Maximum absorption (nm)	Inflection point (nm)	Tentative pigment identification
Trapiche	Green	Cr	Additional file 1: Fig. S1-Cr	Viridian, chrome(III)oxide green and/ or chrome yellow + blue	Additional file 1: Fig. S2-EM2	450, 600, 705	745	Viridian and/or chrome(III)oxide green
	Blue	Co	Additional file 1: Fig. S1-Co	Cobalt blue	Additional file 1: Fig. S2-EM1	540, 580, 630	680	Cobalt blue
	Red	Hg	Additional file 1: Fig. S1-Hg	Vermilion	N/A	N/A	N/A	N/A
	Yellow	Fe	Additional file 1: Fig. S1-Fe	Iron oxide/oxy-hydroxide	Additional file 1: Fig. S2-EM4	630, 900	N/A	Ochre
	Brown				Additional file 1: Fig. S2-EM3			
	Dark/black	Co, Ca	Additional file 1: Fig. S1-Co	Cobalt blue	Additional file 1: Fig. S2-EM5	580, 630	680	Cobalt blue
			Additional file 1: Fig. S1-Ca	Bone black				
	Ground	Pb	Additional file 1: Fig. S1-Pb	Lead white	N/A	N/A	N/A	N/A
CAM-1329	Green	Cr, Co, Zn, As, Cu	Figure 2-Cr	Viridian, chrome(III)oxide green and/ or chrome yellow + blue	Figure 3-EM3–5	450, 600, 705	745	Viridian/ chrome(III)oxide green + ultramarine blue Cobalt blue/Cobalt green Zinc white/Cobalt green
			Figure 2-Co, Zn	Cobalt blue + zinc white and/or cobalt green				
			Figure 2-As, Cu	Emerald and/or Scheele's green	Figure 3-EM7	450, 670		Emerald green
	Blue	N/A	N/A	N/A	Figure 3-EM2	410, 600	690	Ultramarine blue
	Yellow	N/A	N/A	N/A	Figure 3-EM8, EM9	440, 565, 650	500, 695	Possibly organic yellow
	Brown	Hg	Figure 2-Hg	Vermilion	Figure 3-EM6	455, 560, 640	580	Ochre + vermilion
	White	Pb	Figure 2-Pb	Lead white	N/A	N/A	N/A	N/A
	Ground	Pb	Figure 2-Pb	Lead white	N/A	N/A	N/A	N/A
	Retouching	Ca, Fe, K, Ti, Ba	Figure 2-Ca, Fe, Ti, Ba	Calcium carbonate Iron oxide/oxy—hydroxide Titanium white Barium sulfate	Figure 3-EM1	630, 900		Ochre

Vermeulen *et al. Heritage Science*   (2022) 10:44

Page 9 of 22

Table 2 (continued)

Painting	Color	MA-XRF			Reflectance spectroscopy			
		Element	Figure/distribution map	Tentative pigment identification	Distribution map/spectrum	Maximum absorption (nm)	Inflection point (nm)	Tentative pigment identification
CAM-1328	Green	Cu, As, Cr	Additional file 1: Fig. S3-Cu, As	Emerald green and/or Scheele's green	Additional file 1: Fig. S4-EM1	450, 670		Emerald green
			Additional file 1: Fig. S3-Cr	Viridian, chrome(III) oxide green and/or chrome yellow + blue				
	Blue	N/A	N/A	N/A	Additional file 1: Fig. S4-EM5	590	700	Ultramarine blue
	Red	Hg	Additional file 1: Fig. S3-Hg	Vermilion	Additional file 1: Fig. S4-EM7	660	590	Vermilion-containing red
	Yellow	N/A	N/A	N/A	Additional file 1: Fig. S4-EM2, EM3	440	500	Possibly organic yellow
	Brown	Fe, Mn, Hg, Ca	Additional file 1: Fig. S3-Fe, Mn	Umber	Fig. S4-EM6	N/A	700	Unknown brown, most likely containing ultramarine blue
			Additional file 1: Fig. S3-Hg	Vermilion				
			Additional file 1: Fig. S3-Ca	Bone black or calcium carbonate				
	Ground	Pb	Additional file 1: Fig. S3-Pb	Lead white	N/A	N/A	N/A-	N/A
	Retouching	Ca, Fe, K, Ti, Ba, Co, Zn	Additional file 1: Fig. S3-Fe	Iron oxide/oxy-hydroxide	Additional file 1: Fig. S4-EM4	630, 890	520	Ochre
			Additional file 1: Fig. S3-K	Unknown				
			Additional file 1: Fig. S3-Ca	Calcium carbonate				
			Additional file 1: Fig. S3-Ti	Titanium white				
			Additional file 1: Fig. S3-Ba	Barium sulfate				
			Additional file 1: Fig. S3-Co, Zn	Cobalt blue/cobalt green Zinc white/cobalt green				

Vermeulen *et al. Heritage Science* *(2022) 10:44*

Page 10 of 22

Table 2 (continued)

Painting	Color	MA-XRF			Reflectance spectroscopy			
		Element	Figure/ distribution map	Tentative pigment identification	Distribution map/ spectrum	Maximum absorption (nm)	Inflection point (nm)	Tentative pigment identification
2004–005	Green	Cr	Additional file 1: Fig. S5-Cr	Viridian, chrome(III) oxide green and/or chrome yellow + blue	Additional file 1: Fig. S6-EM7	450, 600, 710	750	Viridian and/or chrome(III)oxide green
	Red	Hg	Additional file 1: Fig. S5-Hg	Vermilion	Additional file 1: Fig. S6-EM5, EM6	540, 660, 700	580	Mixture containing vermilion
	Yellow	N/A	N/A	Possibly organic	Additional file 1: Fig. S6-EM1	N/A	N/A	Unknown (possibly organic) yellow
	Brown	Fe, Mn, Hg	Additional file 1: Fig. S5-Fe, Mn	Umber	Additional file 1: Fig. S6-EM2	N/A	N/A	Unknown dark
			Additional file 1: Fig. S5-Hg	Vermilion				
	Black	Cr, Ca, Mn, Hg	Additional file 1: Fig. S5-Cr	Viridian, chrome(III) oxide green and/or chrome yellow + blue	N/A	N/A	N/A	N/A
			Additional file 1: Fig. S5-Ca	Bone black				
			Additional file 1: Fig. S5-Mn	Umber				
			Additional file 1: Fig. S5-Hg	Vermilion				
	Ground	Pb Ca Ba	Additional file 1: Fig. S5-Pb	Lead white Calcium carbonate Barium sulfate	N/A	N/A	N/A	N/A
	Retouching	Ca, Fe, K, Ti, Ba, Co, Zn	Additional file 1: Fig. S5-Mn	Umber	Additional file 1: Fig. S6-EM3	630, 705, 795		Possibly organic green
			Additional file 1: Fig. S5-Ca	Calcium carbonate				
			Additional file 1: Fig. S5-K	Unknown				
			Additional file 1: Fig. S5-Ti	Titanium white	Additional file 1: Fig. S6-EM4	480, 630, 890		Ochre
			Additional file 1: Fig. S5-Ba	Barium sulfate				
			Additional file 1: Fig. S5-Co, Zn	Cobalt blue/ cobalt green Zinc white/ cobalt green				

Vermeulen *et al. Heritage Science*   *(2022) 10:44*

Page 11 of 22

Table 2 (continued)

Painting	Color	MA-XRF			Reflectance spectroscopy			
		Element	Figure/ distribution map	Tentative pigment identification	Distribution map/ spectrum	Maximum absorption (nm)	Inflection point (nm)	Tentative pigment identification
2004–007	Green	Cu, As, Cr	Additional file 1: Fig. S7-Cu, As	Emerald green and/or Scheele's green	Additional file 1: Fig. S8-EM2	430, 680		Emerald green
			Additional file 1: Fig. S7-Cr	Viridian, chrome(III) oxide green and/or chrome yellow + blue	Additional file 1: Fig. S8-EM7	680	480	Prussian blue + yellow
	Blue	N/A	N/A	N/A	Additional file 1: Fig. S8-EM1	680		Prussian blue
	Red	Hg	Additional file 1: Fig. S7-Hg	Vermilion	Additional file 1: Fig. S8-EM8	N/A	590	Vermilion
	Yellow	Cr	Additional file 1: Fig. S7-Cr	Chrome yellow	N/A	N/A	N/A	N/A
	Brown	Fe, Mn	Additional file 1: Fig. S7-Fe, Mn	Umber	Additional file 1: Fig. S8-EM3, EM4	690	575	Unknown
	Black	Ca, Co	Additional file 1: Fig. S7-Ca	Bone black	Additional file 1: Fig. S8-EM5	N/A	N/A	Unknown
			Additional file 1: Fig. S7-Co	Cobalt blue				
	Ground	Pb, Ba, Zn, Ca, S	Additional file 1: Fig. S7-Pb	Lead white	N/A	N/A	N/A	N/A
			Additional file 1: Fig. S7-Ba	Barium sulfate				
			Additional file 1: Fig. S7-Zn	Zinc oxide				
			Additional file 1: Fig. S7-Ca	Calcium carbonate and/ or sulfate				
	Possible retouching	Zn	Additional file 1: Fig. S7-Zn	Zinc white	Additional file 1: Fig. S8-EM6	630, 710, 795		Possibly modern pigment

Vermeulen *et al. Heritage Science*   (2022) 10:44

Page 12 of 22

Table 2 (continued)

Painting	Color	MA-XRF			Reflectance spectroscopy			
		Element	Figure/ distribution map	Tentative pigment identification	Distribution map/ spectrum	Maximum absorption (nm)	Inflection point (nm)	Tentative pigment identification
2003–05–02	Green	Cr, Cu	Additional file 1: Fig. S9-Cr	Viridian, chrome(III) oxide green and/or chrome yellow + blue	Additional file 1: Fig. S10-EM4	700	505	Prussian blue + yellow
			Additional file 1: Fig. S9-Cu	Cu-based green such as verdigris, copper resinate or malachite				
	Blue	N/A	N/A	N/A	Additional file 1: Fig. S10-EM1	700	N/A	Prussian blue
					Additional file 1: Fig. S10-EM3	420, 600	720	Ultramarine blue
	Red	Fe, Hg	Additional file 1: Fig. S9-Fe	Iron oxide/oxy-hydroxide	Additional file 1: Fig. S10-EM2	480, 650, 865	580	Red ochre
			Additional file 1: Fig. S9-Hg	Vermilion	Additional file 1: Fig. S10-EM5	485, 650, 900	585	Vermilion (+ iron oxide)
	Yellow	Fe, Cr	Additional file 1: Fig. S9-Fe	Iron oxide/oxy-hydroxide	Additional file 1: Fig. S10-EM6	555, 620, 850	N/A	Yellow ochre + other yellow
			Additional file 1: Fig. S9-Cr	Chrome yellow	Additional file 1: Fig. S10-EM8	480, 620	520	Possibly chrome yellow
	Brown	Fe, Mn	Additional file 1: Fig. S9-Fe, Mn	Umber				
	Black	Ca	Fig. S9-Ca	Bone black	Additional file 1: Fig. S10-EM9	645	N/A	Bone black
	Ground	Pb Zn	Additional file 1: Fig. S9-Pb	Lead white Zinc white	N/A	N/A	N/A	

(Fig. 3-EM7 and Additional file 1: Fig. S4-EM1), despite the technique not being suitable to differentiate the two pigments. In the case of 2004–007, RIS did not allow for the identification of the pigment due to its color being too dark to return any usable features, highlighting some of the limitations of non-invasive imaging techniques.

Despite not being identified by MA-XRF due to its constituting elements being too light to be picked up by the technique, RIS highlighted the use of ultramarine blue (sulfur-containing sodium aluminum silicate) in the blue highlights (Fig. 3-EM2) as well as in the blue pillow in 2003–05–02 (Additional file 1: Fig. S10-EM3). Co, an element often associated with cobalt blue [cobalt(II) oxide-aluminum oxide], was identified by MA-XRF in the green areas of the guanábanas (Fig. 2-Co). The Co was observed in association with Zn (Fig. 2-Zn), which may suggest a combined used of cobalt blue and zinc white (zinc oxide). However, this association would prove peculiar due to the rather dark color of the depicted fruit, for which zinc white would not be expected.

Furthermore, the co-presence of Co and Zn may also be associated with a cobalt green: a cobalt oxide-doped zinc oxide pigment. Even though it was not possible to confirm the presence of the pigment using minimally invasive techniques due to the lack of sample in the area, cobalt green was identified with Raman spectroscopy in the light blue sky of Trapiche Meladero (see section "Micro-invasive investigation: optical microscopy, SEM–EDX, and Raman spectroscopy"), another of Oller's painting for which Co and Zn were identified using MA-XRF (Additional file 1: Fig. S1). This finding may support the possible use of the pigment in this second painting by the same artist.

The presence of Zn and Cr in the guanábanas could also be associated with the use of yellow zinc chromate. However, both elements do not seem to overlap contrary to Co and Zn as suggested by the RGB composite images presented in Fig. 4, and therefore, supporting further the use of cobalt green and/or a mixture of cobalt blue and zinc white.
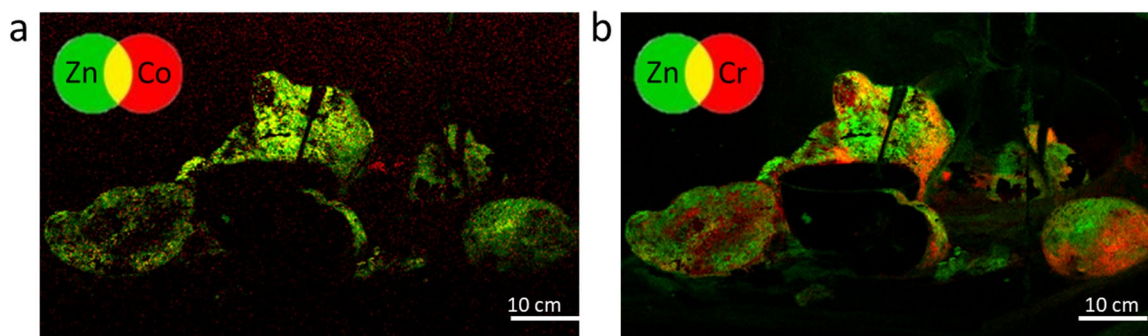
Fig. 4 RGB composite images for **a** Co (red) and Zn (green) and **b** Cr (red) and Zn (green) highlighting the elemental overlap of Co and Zn (yellow) rather than Cr and Zn in CAM-1329. The nearly perfect Co/Zn overlap suggests the use of cobalt green and/or cobalt blue and zinc white mixture rather than the use of zinc chromate

Except for the warm background, yellow tones are only sparsely used throughout the composition of CAM-1329. Yellow is mostly observed in the yellow knife handle and in the light-yellow filling of the bowl. Neither these elements nor the background yields any elemental response that could be linked to yellow pigments, such as Cr (for chrome or lemon yellows), often identified in paintings from impressionist and post-impressionist periods. RIS, while not able to identify the pigment used, did however set apart both areas (Fig. 3-EM8, 9 for the knife handle and background, respectively), with features at 565 and 650 nm possibly associated with an ochre pigment, not identified through the presence of Fe in MA-XRF. The lack of elemental response in the yellow areas may suggest the use of organic lakes and/or synthetic organic pigments, further suggested by the absorbance band at 440 nm observed in RIS (Fig. 3-EM8, 9). Similar observations can be made for the knife handle, avocado flesh, and background of CAM-1328 (Additional file 1: Figs. S3, S4). Nonetheless, non-invasive imaging techniques do not enable most yellow colorants to be identified and further analyses more suited for the identification of organic pigments such as Raman spectroscopy or LCMS are necessary (section "Micro-invasive chromatographic analysis: HPLC–DAD-MS/MS").

Micro-invasive investigation: optical microscopy, SEM–EDX, and Raman spectroscopy

Optical microscopy, SEM-EDX mappings and Raman spectroscopy undertaken on embedded samples allowed for a better understanding of the paint stratigraphy as well as the distribution of the pigments and their identification. SEM-EDX and Raman allowed for the confirmation of the pigments tentatively identified using non-invasive imaging techniques and reported in Table 2 along with gaining insights into the nature of the ground used by the artists.

The sample taken from the light blue sky of Trapiche Meladero presents Co/Al-rich blue and Co/Zn-rich green coarse pigment particles dispersed in a Pb-rich white matrix (Fig. 5). Using Raman spectroscopy, the Pb-rich white matrix was identified as lead white through its bands at 1050 cm^{-1} (Fig. 6a), whereas the Co/Zn-rich green and the Co/Al-rich blue particles were identified as cobalt green (Fig. 6a) and cobalt blue (Fig. 6b), respectively (Table 3). The positive identification of Co/Zn-rich cobalt green in mixture with a blue pigment in Trapiche Meladero could support the use of the same cobalt green pigment in mixture with Cr-based and Cu-based green hypothesized in CAM-1329 (see section "Non-invasive imaging techniques: MA-XRF and RIS").

While inferred with MA-XRF and SEM-EDX (Additional file 1: Fig. S3 and Fig. 7), a lead white ground was identified in the cross-section taken from CAM-1328 based on its 1050 cm^{-1} characteristic Raman band (Fig. 6c). Furthermore, Cr-based and Cu/As-based greens, also inferred using non-invasive imaging spectroscopies, were also observed with SEM-EDX in the green particles of CS2 (Fig. 7). These pigments were then respectively identified as viridian (Fig. 6d) and Emerald green (Fig. 6e) based on their characteristic Raman shift reported in Table 3. Though viridian refers to the hydrated chrome oxide form ($Cr_2O_3 \cdot 2H_2O$), the spectrum reported in Fig. 6d presents bands characteristic for both the hydrated (viridian; 583, 487 and 260 cm^{-1}) and the anhydrous oxide [chrome(III) oxide, 541 and 345 cm^{-1}]. Such features for viridian have been reported before [40].

Both techniques also allowed for the identification of ultramarine blue, based on the presence of Al and Si in the EDX spectrum (Fig. 7) and its 256, 546 and 804 cm^{-1} vibration bands in the Raman spectrum (Fig. 6f). Vermilion was confirmed in the red particles (not observed with SEM-EDX but identified by Raman through the 252, 284 and 342 cm^{-1} characteristic bands, Fig. 6g).
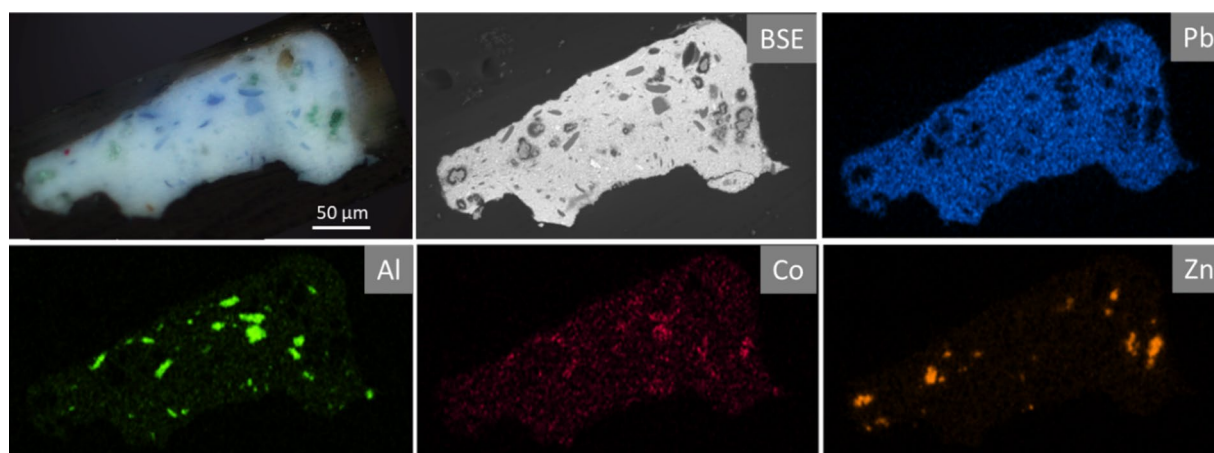
Fig. 5 Visible light image of CS1, SEM backscattered electron image and Pb, Al, Co and Zn elemental maps highlighting the use of cobalt green (Co/Zn) along with cobalt blue (Co/Al) and lead white (Pb) in the light blue sky of Oller's Trapiche Meladero

Raman shifts, elements detected using SEM-EDX, and the associated pigment identifications for all five cross-sections investigated are summarized in Table 3.
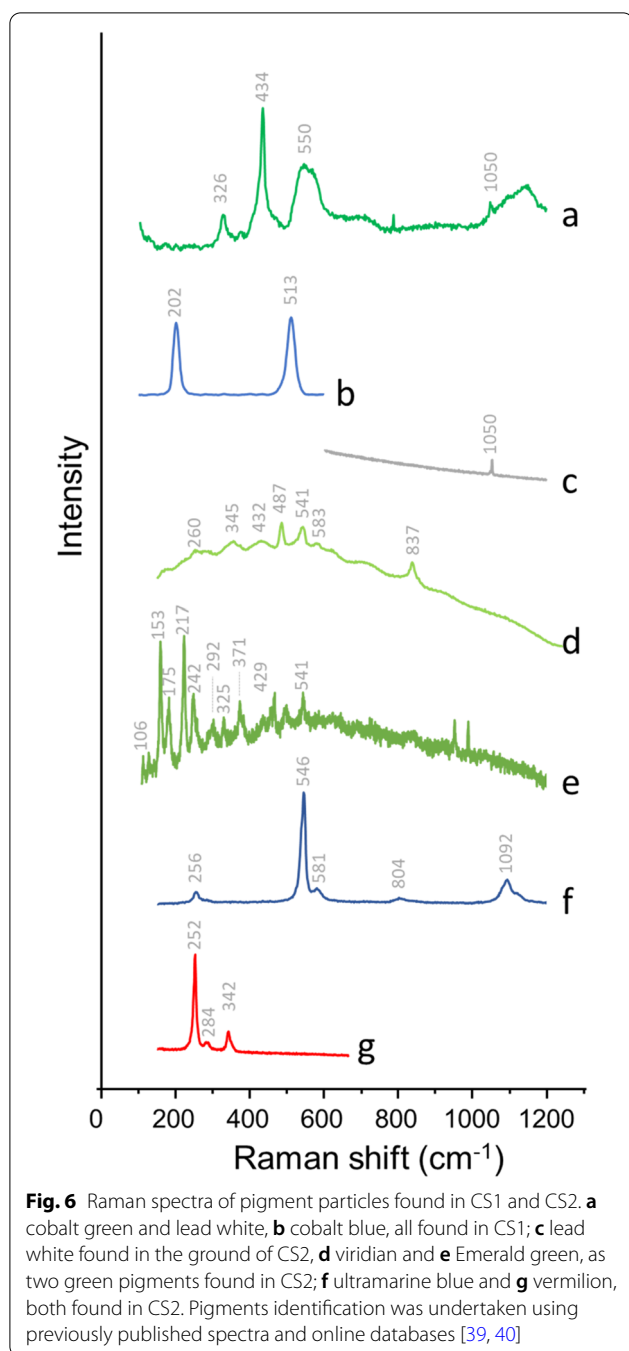
The yellow area of CS2 (Fig. 7) did not yield any elemental response expected for inorganic yellow pigments such as Cr or Zn. A similar observation was made for CS3 (Additional file 1: Fig. S11) for which the lower darker reddish-yellow layer contained iron and was identified as Mars red by Raman (Additional file 1: Fig. S14a) whereas the upper light-yellow layer only contained Ba and could not be identified with spectroscopic techniques (Additional file 1: Fig. S11). The yellow colors found in Oller's paintings, which did not present any elemental response in MA-XRF (knife handle, avocado flesh, bowl content, Fig. 2, and Additional file 1: Fig. S3) were further investigated using the scrapings taken in the above-mentioned areas (Fig. 1). The SEM–EDX from the knife handle showed a mixture of Pb and Ba (data not shown) but confirmed the lack of elements usually associated with inorganic yellow, further suggesting the use of an organic yellow pigment or lake. However, Raman spectroscopy, which is well suited for the investigation of synthetic organic pigments [41–43], did not produce any spectra which would enable the pigments/colorants to be identified. This further emphasized the need for additional analysis using HPLC-DAD-MS/MS.

Micro-invasive chromatographic analysis: HPLC–DAD-MS/MS

The two yellow samples (SCR2 and SCR3) analyzed by HPLC-DAD-MS/MS revealed the use of two synthetic organic pigments in paintings CAM-1329 and CAM-1328.

For sample SCR2 (CAM-1329) the DAD chromatogram acquired at 350 nm showed a single peak at ca. 9.8 min (Fig. 8a), corresponding to a compound with a characteristic UV–Vis absorption spectrum showing two distinct absorption maxima at ca. 340 and 410 nm (Fig. 8a—insert). The mass spectrometric data revealed that the compound produced a positive ion $[M+H]^+$ at *m/z* 341.124 (Fig. 8b), but no clear mass was detected in negative ionization mode. The tandem mass spectrum was recorded in positive ionization mode (Fig. 8c). The results, specifically the retention time, UV–Vis absorption spectrum, accurate mass and tandem mass spectrum, were in perfect agreement with the analyses carried out on a reference sample of PY1 (Hansa Yellow G—C.I. 11680). The molecule ionizes in negative mode as well, producing a $[M-H]^-$ ion at *m/z* 339.110, although the intensity of the negative ion is lower than the intensity of the corresponding positive ion. This explains the result obtained for sample SCR2, as the concentration of the molecule extracted from the tiny sample was not sufficient to produce a detectable negative ion. The results obtained for the reference sample of PY1, including the tandem mass spectrum obtained in negative ionization mode, are reported in Supplementary Information (Additional file 1: Fig. S15) together with a brief discussion of the mass fragmentations observed in both positive and negative ionization modes.

For sample SCR3 (CAM-1328) the DAD chromatogram acquired at 350 nm showed a single peak at ca. 10.4 min (Fig. 9a), corresponding to a compound with a very similar UV–Vis absorption spectrum to what observed for sample SCR2, also showing two distinct

Vermeulen *et al. Heritage Science*   (2022) 10:44

Page 15 of 22

Fig. 6 Raman spectra of pigment particles found in CS1 and CS2. **a** cobalt green and lead white, **b** cobalt blue, all found in CS1; **c** lead white found in the ground of CS2; **d** viridian and **e** Emerald green, as two green pigments found in CS2; **f** ultramarine blue and **g** vermilion, both found in CS2. Pigments identification was undertaken using previously published spectra and online databases [39, 40]

with the analyses carried out on a reference sample of PY3 (Hansa Yellow 10G—C.I. 11710). Similarly to PY1, the molecule ionizes in negative mode as well, producing a $[M-H]^-$ ion at *m/z* 393.016, with a lower intensity compared to the positive ion, again explaining the lack of detection of the deprotonated molecule in sample SCR3, due to a very low concentration. The results obtained for the reference sample of PY3, including the tandem mass spectrum obtained in negative ionization mode, are reported in Supplementary Information (Additional file 1: Fig. S16) together with a brief discussion of the mass fragmentations observed in both positive and negative ionization modes.

Discussion

Most of the pigments used by Oller, Cuchí y Arnau, and Frade and identified during this study are similar to the ones used by French and American impressionist and post-impressionist artists of the time [6, 7, 9, 10, 36, 44–49]. As described in the results section and summarized in Tables 2 and 3, these pigments include hydrated chromium oxide (known as viridian), and Emerald green for the greens; Prussian blue, cobalt blue and ultramarine blue for the blues; vermilion and red ochre for the reds and skin tones; yellow ochres and chrome yellow for the yellows; umber or sienna for the browns; cobalt blue and possibly bone/ivory black as constituents of the darker and black passages. Lead and zinc were identified in white areas and indicate the use of lead white and zinc white, respectively. Mixtures of aforementioned pigments have been identified and are reported in Table 2. Green pigments such as viridian and Emerald green are often reported in technical studies of impressionist and post-impressionist artists such as Monet, Renoir, Pissarro, and Munch. This is to be expected as these pigments are often listed in major paint manufacturing companies such as Winsor & Newton, Bourgeois Ainé, and Lefranc [50]. Consequently, due to their ties with European artists, such pigments could be expected as part of the Puerto Rican artists' palettes. Despite the large correspondence between pigments used by these three Puerto Rican artists and their European and American contemporaries, both non-invasive and minimally invasive analyses highlighted the use of cobalt green and synthetic organic yellows, pigments usually not reported in technical studies of paintings from this time period.

The use of cobalt green, a cobalt oxide-doped zinc oxide green pigment, appears unexpected. Indeed, while invented in 1780 by Swedish Chemist Sven Rinmann, the pigment is rarely reported in technical studies of late nineteenth century artists. Despite its permanence, the pigment was unpopular upon its discovery due to its high cost and poor tinting strength [51]. It was described

absorption maxima at ca. 340 and 410 nm (Fig. 9a—insert). In addition to the different retention time, the compound produced a positive ion $[M+H]^+$ at *m/z* 395.031 (Fig. 9b). Also in this case, no clear mass was detected in negative ionization mode. The tandem mass spectrum was therefore recorded in positive ionization mode (Fig. 9c). The results, specifically the retention time, UV–Vis absorption spectrum, accurate mass and tandem mass spectrum, were in perfect agreement

Vermeulen *et al. Heritage Science*   (2022) 10:44

Page 16 of 22

Table 3 Overview of the materials identified through minimally invasive analyses of the six investigated paintings

Painting	Sample	Analytical technique and associated element (SEM-EDX) and Raman shifts (cm^{-1})		Figure	Identified materials in ground and colored layers
Trapiche	CS1	SEM-EDX	Co, Al, Zn, Pb	Figure 5	Ground: N/A Colored layer: cobalt blue, cobalt green and lead white
		Raman	328, 434, 545, 567, 1050, 1090–1142	Figure 6a	
			202, 513	Figure 6b	
CAM-1329	SCR1	SEM-EDX	Pb, Ba	N/A	Ground: N/A Colored layer: lead white, vermilion, and Ba-containing yellow, likely organic, identified as PY1 (Hansa Yellow G—C.I. 11680)
		Raman	1050	Additional file 1: Fig. S14j	
			250, 281, 340	Additional file 1: Fig. S14k	
	SCR2	HPLC-DAD-MS/MS		Figure 8	
CAM-1328	CS2	SEM-EDX	Pb, Cr, Cu, As, Ca, Al, Mg	Figure 7	Ground: lead white Colored layer: ultramarine blue, viridian, Emerald green, and vermilion
		Raman	1050	Figure 6c	
			260, 345, 432, 487, 541, 583, 837	Figure 6d	
			106, 153, 175, 217, 242, 292, 325, 371, 429, 541	Figure 6e	
			256, 546, 581, 804, 1092	Figure 6f	
			252, 284, 342	Figure 6g	
	SCR3	HPLC-DAD-MS/MS		Figure 9	PY3 (Hansa Yellow 10G—C.I. 11710)
2004–005	CS3	SEM-EDX	Ba, Ca, Pb, Fe	Additional file 1: Fig. S11	Ground: likely lead white, likely calcium carbonate, and barium sulfate Pigmented layer 1 (top): ba-rich light yellow Pigmented layer 1 (bottom): mars red
		Raman	224, 290, 410, 496, 610	Additional file 1: Fig. S14a	
			453, 461, 986	Additional file 1: Fig. S14b	
2004–007	CS4	SEM-EDX,	Ground: Zn, Ba, S, Ca, Pb, Si Colored layer: Pb, Hg, S	Additional file 1: Fig. S12	Ground: lead white, calcium carbonate, calcium sulfate, quartz, and lithopone Colored layer: lead white, Prussian blue, and vermilion
		Raman	453, 986	Additional file 1: Fig. S14c	
			250, 281, 340	Additional file 1: Fig. S14d	
			154, 281, 1085	Additional file 1: Fig. S14e	
			127, 202, 463	Additional file 1: Fig. S14f	
			1006	Additional file 1: Fig. S14g	
2003–05–02	CS5	SEM-EDX	Pb, Zn, Fe, Al	Additional file 1: Fig. S13	Ground: lead white and zinc white, with inclusion of yellow ochre/goethite Colored layer: N/A
		Raman	1050	Additional file 1: Fig. S14h	
			250, 300, 387	Additional file 1: Fig. S14i	

as "chemically good and artistically bad", which may explain its apparent restricted use in impressionist and post-impressionist paintings. Despite the overall lack of identification in technical studies, cobalt green was recently found in paintings by French artist James Tissot [52]. Furthermore, the pigment was also advertised as part of the pigment catalogue of major paint manufacturing companies such as Winsor & Newton, Bourgeois Ainé, and Lefranc, which confirms its availability to artists [50]. Therefore, its use in late nineteenth century paintings may be more widespread than anticipated and its lack of identification may be attributed to the limitations of non-invasive techniques such as XRF or reflectance spectroscopy. Indeed, with the aforementioned techniques, the pigment may be mistaken for a mixture of zinc white and cobalt blue, two common pigments of this time period. More technical studies of impressionists and post-impressionist paintings with non-invasive and

minimally invasive techniques would be require to confirm this hypothesis. This is however outside of the scope of this article.

The use of synthetic yellow pigments in CAM-1328 and CAM-1329, hypothesized upon non-invasive analyses, and identified with HPLC-DAD-MS/MS as PY1 (Hansa Yellow G—C.I. 11680) and PY3 (Hansa Yellow 10G—C.I. 11710) was also unexpected. Indeed, chrome yellow, cadmium yellow, iron oxide, zinc yellow, strontium yellow, barium yellow and Naples yellow, all widely available from major paint manufacturing companies [50] were often identified in paintings from this time period [7, 44, 47, 53]. In that regard, the use of chrome yellow in in 2004–007 and 2003–05–02 (Additional file 1: Fig. S7, and Fig. S9) corresponds better to the European practices of this time period. Nonetheless, the use of synthetic organic pigments cannot be excluded in late-19th/early twentieth century paintings as this period saw the
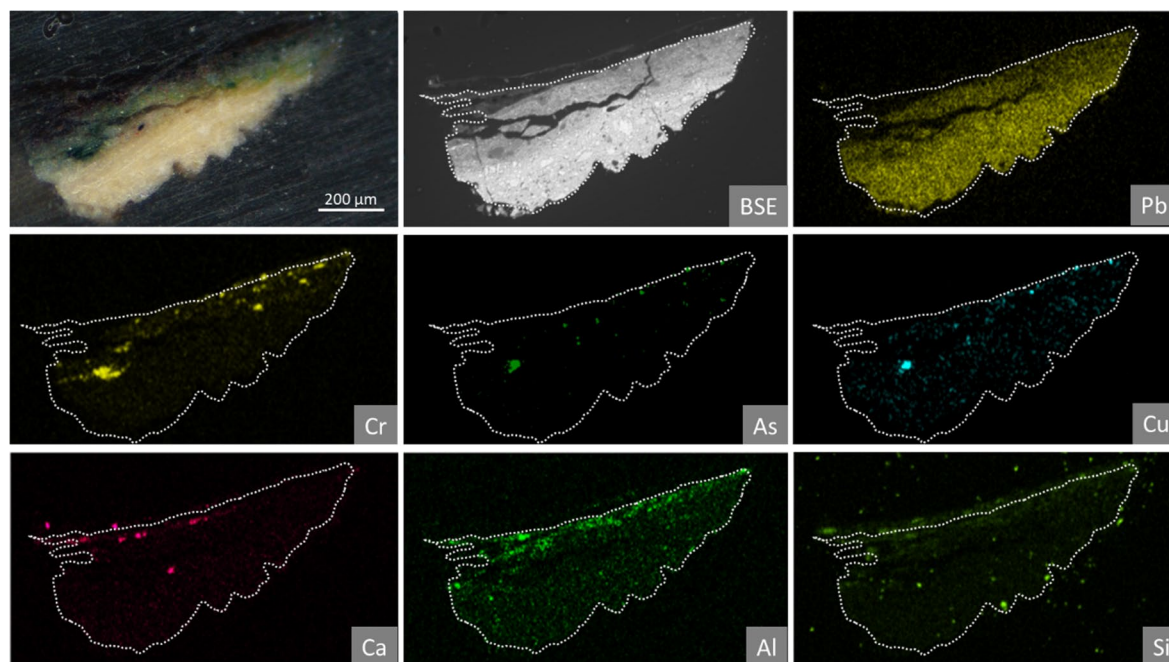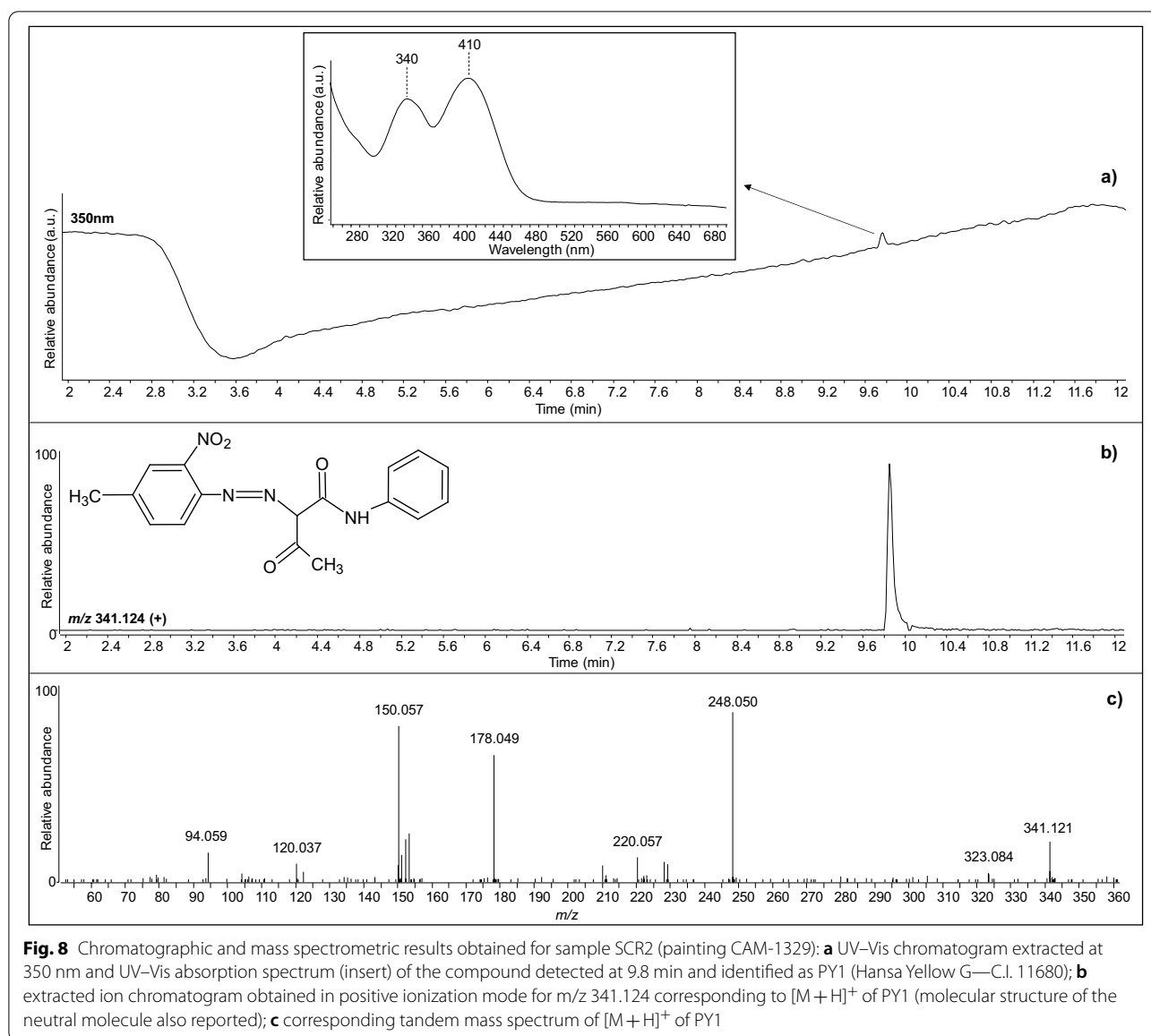
Vermeulen *et al. Heritage Science*   *(2022) 10:44*

Page 17 of 22

Fig. 7 Visible light image, backscattered electron SEM image and EDX elemental distribution maps obtained on CS2. Images and SEM-EDX analyses suggest the presence of a lead white (Pb) ground, followed by a Cr- and Cu/As-containing green layer. The presence of Al and Si in the upper layer also suggest the presence of ultramarine blue. The yellow areas of the sample did not yield any elemental response that would allow to identify the yellow pigment, which may suggest the use of an organic yellow pigment

development of many organic pigments. This includes some organic yellows such as tartrazine (PY100—C.I. 19140:1), discovered in 1884 by H. Ziegleras [51, 54] as well as several Hansa yellows in the early 1900s [43, 54]. Both PY1 and PY3 are described as light-valued opaque to semitransparent intense yellows, therefore making them suitable alternative to bright chrome yellow [55]. PY3, identified in the avocado flesh of CAM-1328, is also described as bright greenish yellow [54], making it suitable to depict the greenish hue of the avocado flesh. While both PY1 and PY3 may not appear as immediate candidates to impressionist and post-impressionist paintings, they were respectively discovered in 1909–10 and 1910–11 [54, 56] and started to be produced in 1910 [56], therefore during the lifetime of Francisco Oller (1833–1917).

Despite the current lack of historical information, it is known that Ricardo Alegría (1921–2011)—a Puerto Rican historian, cultural anthropologist and archaeologist—and Osiris Delgado (1920–2017)—a painter, writer, and art historian also from Puerto Rico—used biographical and historical data to date the paintings from circa 1890 (CAM-1329) and 1890–91 (CAM-1328), as indicated in the museum's records. This approach therefore dated the paintings 20 years prior to the discovery and development of PY1 and PY3. Nonetheless, the pigments were available prior to Oller's death in 1917, with the artist known for having been active until the end of his life creating paintings such as Guayabas being dated 1901–03; Higueras being dated ca. 1912; and Piñas dated 1912–14 [57]. Furthermore, close visual examinations do not present signs of losses and overpaints in the yellow areas analyzed, suggesting the yellows areas to be original. As a result, the presence of these pigments (PY1 and PY3) allows us to change the terminus post quem of CAM-1328 and CAM-1329 to 1910, further emphasizing Oller's activity until late in his career. This also illustrates the importance of scientific analyses along with the connoisseurship approach to better comprehend the history associated with artworks, especially when these are not explicitly dated. When combined, both approaches help
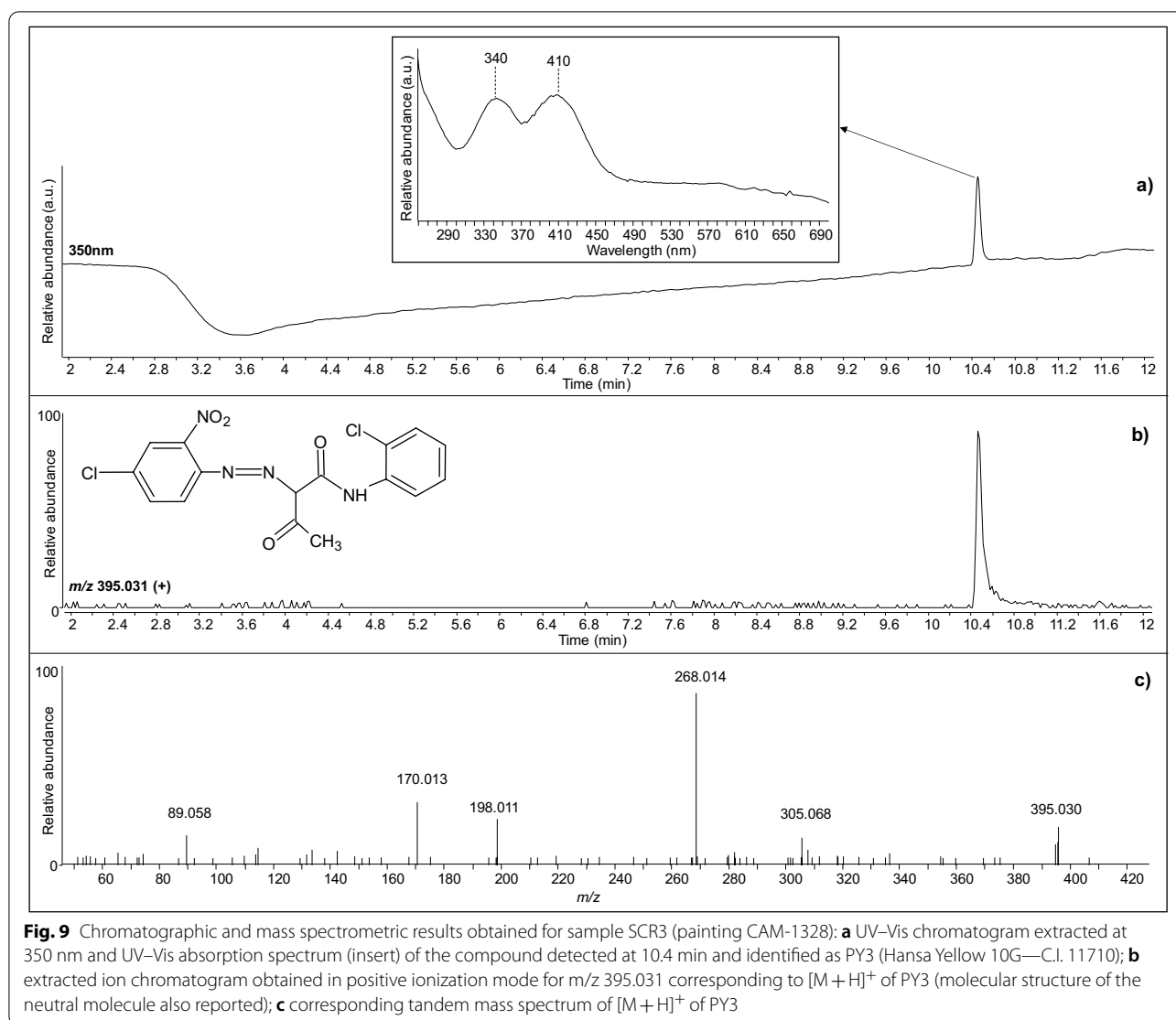
Vermeulen *et al. Heritage Science*   (2022) 10:44

Page 18 of 22

Fig. 8 Chromatographic and mass spectrometric results obtained for sample SCR2 (painting CAM-1329): **a** UV–Vis chromatogram extracted at 350 nm and UV–Vis absorption spectrum (insert) of the compound detected at 9.8 min and identified as PY1 (Hansa Yellow G—C.I. 11680); **b** extracted ion chromatogram obtained in positive ionization mode for m/z 341.124 corresponding to [M + H]$^+$ of PY1 (molecular structure of the neutral molecule also reported); **c** corresponding tandem mass spectrum of [M + H]$^+$ of PY1

refine the information associated with the artwork, which is then made available to scholars and the wider public.

Conclusions

This technical study aimed to characterize Impressionist and Post-Impressionist Puerto Rican artists' palettes for the first time. Due to the relationship Puerto Rico had with Europe until the late nineteenth century and the transatlantic travels of the Puerto Rican artists, they are key figures to help understand the influence of European practices in the Caribbean. Non-invasive techniques (namely MA-XRF and RIS), coupled with complementary minimally invasive techniques such as

SEM-EDX, Raman and HPLC-DAD-MS/MS allowed for the characterization of the artists' palettes. While these artists used pigments traditionally employed in the late nineteenth century (lead white, zinc white, cobalt blue, Prussian blue, ultramarine blue, Emerald green, viridian, vermilion, red iron oxide, umber, yellow iron oxide, chrome yellow, bone black), this study highlighted the use of organic yellow pigments (PY1 and PY3) and cobalt green, a notoriously expensive and unpopular pigment due to its poor tinting strength. The use of organic yellows instead of usual inorganic yellow pigments is unexpected, as they are rarely found in technical studies of late 19th/early twentieth century

Vermeulen *et al. Heritage Science*   (2022) 10:44

Page 19 of 22

Fig. 9 Chromatographic and mass spectrometric results obtained for sample SCR3 (painting CAM-1328): **a** UV–Vis chromatogram extracted at 350 nm and UV–Vis absorption spectrum (insert) of the compound detected at 10.4 min and identified as PY3 (Hansa Yellow 10G—C.I. 11710); **b** extracted ion chromatogram obtained in positive ionization mode for m/z 395.031 corresponding to [M + H]$^+$ of PY3 (molecular structure of the neutral molecule also reported); **c** corresponding tandem mass spectrum of [M + H]$^+$ of PY3

paintings and inorganic yellow pigments were widely available from paint manufacturers. The use of PY1 and PY3, with well documented discovery and production dates, also allowed to redefine the realization dates of the two paintings in which they were found from 1890–91 to post-1910, closer to the end of Francisco Oller's career. Finally, cobalt green, while hitherto never identified in technical studies of impressionist and post-impressionist paintings, was identified in two successive NU-ACCESS projects. This may indicate that it was more widely used than one would think, but its identification went undetected due to the pigment sharing its elemental constitution with cobalt blue and zinc white,

widely used at the time. These results clearly support the importance of integrated studies including non-invasive, imaging techniques along with minimally invasive molecular techniques, thus providing a full understanding of the nature and spatial distribution of inorganic and organic materials used in paintings.

Abbreviations
MA-XRF: Macro-X-ray fluorescence; RIS: Reflectance imaging spectroscopy; BSE: Backscattered electron; SEM-EDX: Scanning electron microscopy coupled to energy dispersive X-ray spectrometry; HPLC-DAD-MS/MS: High pressure liquid chromatography coupled to diode array detector and tandem mass spectrometry.

Supplementary Information

The online version contains supplementary material available at https://doi.org/10.1186/s40494-022-00683-9.

Additional file 1: Table S1. Per pixel acquisition time (s), step size (mm) and number of scans associated with all paintings analyzed. **Figure S1.** Registered RGB and MA-XRF elemental maps (greyscale), obtained for Trapiche Meladero. Elemental distribution maps suggest the use of a lead-based pigment (probably lead white, Pb); iron-based yellow and brown ochres (Fe); Ni-containing cobalt-based pigment (Ni, Co); Ca- and Co-containing black (likely to be a mixture of bone black and cobalt blue; Ca, Co); vermilion (Hg); chrome-based green, likely to be viridian or chrome oxide green (Cr); and zinc-containing pigment (Zn). **Figure S2.** Registered RGB, RIS distribution maps (colored) and associated reflectance curves obtained for Trapiche Meladero. RIS distribution maps suggest the use of cobalt blue (EM1); chrome-based green, likely to be viridian or chrome oxide green (EM2); iron-oxide yellow and brown (EM3 and EM4) and Co bluecontaining black (EM5). Threshold and minimum distance values of respectively 0.1 and 15 were used for the RIS endmembers extraction procedure. **Figure S3.** Registered RGB, and MA-XRF elemental maps (greyscale obtained for CAM-1328. Elemental maps for Fe, Ca, Ti, Zn, Ba and Co appear to be associated with conservation intervention whereas Pb, Cu, As, Cr, Hg, K, Mn, and some Fe appear associated with the original paint layer. Elemental distribution maps suggest the use of a lead-based ground (likely to be lead white, Pb); Emerald/Scheele's green (Cu/As); chrome-based green (Cr); iron oxide-based ochres including umber (Fe, Mn); possibly a vermilioncontaining dark pigment mixture (Hg. MA-XRF lacks elemental responses for blues and yellows. **Figure S4.** Registered RGB, RIS distribution maps (colored) and associated reflectance curves obtained for CAM-1328. RIS distribution maps suggest the use of a Emerald/Scheele's type green (EM1); unknown yellows (EM2 and EM3); an iron oxide-based conservation intervention (EM4); ultramarine blue (EM5); possibly vermilion/ultramarine blue dark pigment mixture (EM6) and vermilion (EM7). Threshold and minimum distance values of respectively 0.1 and 15 were used for the endmembers extraction procedure. **Figure S5.** Registered RGB, and MA-XRF elemental maps (greyscale) obtained for 2004.005. Elemental maps for Ba, Zn, Co, part of Ca and Fe appear to be associated with conservation intervention whereas Pb, Hg, Cr, Mn and part of Fe appear associated with the original paint layer. Elemental distribution maps suggest the use of a lead-based pigment (probably lead white, Pb); vermilion (Hg); Cr-based green (possibly viridian or chrome(III)oxide green, Cr); possibly iron oxide-containing ochres and/or umber type pigments (Fe, Mn). **Figure S6.** Registered RGB, RIS distribution maps (colored) and associated reflectance curves obtained for 2004.005. RIS distribution maps suggest the use of a an unknown yellow (EM1), an unknown dark (EM2), an unknown green (EM3, probably a conservation intervention); a vermilion-containing mixtures (EM5 and EM6) and possibly viridian or chrome(III)oxide green (EM7). Threshold and minimum distance values of respectively 0.1 and 15 were used for the endmembers extraction procedure. **Figure S7.** MA-XRF elemental maps obtained for 2004–007. Elemental distributions suggest the use of barium sulfate (Ba), calcium carbonate (Ca), cobalt blue (Co), chrome yellow (Cr) lead white (Pb), iron oxide (Fe), vermilion (Hg), umber type pigment (Mn/Fe), zinc white (Zn) and Emerald green (Cu/As). Most elements appear associated with the original paint layer. **Figure S8.** RIS distribution maps and associated reflectance curves obtained for 2004–007. Reflectance spectroscopy suggests the use of Prussian blue (EM1), Emerald green (EM2), unknown dark areas (EM3, EM4, EM5), unknown pigment (EM6), Prussian blue-containing green (EM7), and vermilion-containing reds (EM8). **Figure S9.** Registered RGB, and MA-XRF elemental maps (greyscale) obtained for 2003–05–02. All elemental maps appear to be associated with original paint layer. The Mn-free Fe present where Pb is lacking in the cushion may be associated with a pentimenti. Elemental distribution maps suggest the use of a lead-based pigment (probably lead white, Pb); zinc-based pigment (likely zinc white); vermilion (Hg); Cr-based green [possibly viridian or chrome(III)oxide green, Cr]; possibly iron oxide-containing ochres and/or umber type pigments (Fe, Mn). **Figure S10.** RIS distribution maps and associated reflectance curves obtained for 2003–05–02. Reflectance spectroscopy suggests the use of Prussian blue (EM1), iron oxide red (EM2), ultramarine blue (EM3), unidentified green (EM4), mixture of vermilion and iron oxide (EM5), iron oxide-containing yellow mixture (EM6), unknown white (EM7), unknown yellow (EM8) and unknown brown (EM9). **Figure S11.** Visible light image, BSE SEM image and EDX elemental distribution maps obtained on CS3. Images and SEM-EDX analyses suggest the presence of 4 layers: (1) a Ba/Ca/Pb ground; (2) a warm calcium-rich layer; (3) a thin iron oxide yellow layer, and (4) a thicker light yellow, low Z element top layer. **Figure S12.** Visible light image, BSE SEM image and EDX elemental distribution maps obtained on CS4. Images and SEM-EDX analyses suggest the presence of a lead white)/zinc white/calcium carbonate/barium sulfate ground (Pb/Zn/Ca/Ba), followed by a vermilion and lead white-rich upper layer (Hg/S/Pb). **Figure S13.** Visible light image, BSE SEM image and EDX elemental distribution maps obtained on CS5. Images and SEM-EDX analyses suggest the presence of lead white and zinc white mixed ground with small inclusions of Al-based pigment particles. **Figure S14.** Raman spectra for pigment particles found in **a**, **b** CS3, **c**–**g** CS4, **h**, **i** CS5, (**j**, **k** SCR1. **a** Mars red, **b** barium sulfate, **c** barium sulfate, **d** vermilion, **e** calcium carbonate, **f** quartz, **g** calcium sulfate, **h** lead white, **i** yellow ochre/goethite, **j** lead white, and **k** vermilion. **Figure S15.** Chromatographic and mass spectrometric results obtained for the reference sample of PY1: **a** UV–Vis chromatogram extracted at 350 nm and UV–Vis absorption spectrum (insert); **b** tandem mass spectrum obtained in positive ionization mode and proposed justification of fragment ions; **c** tandem mass spectrum obtained in negative ionization mode and proposed justification of fragment ions. The position of the charges on the molecular structures is only indicative. **Figure S16.** Chromatographic and mass spectrometric results obtained for the reference sample of PY3: **a** UV–Vis chromatogram extracted at 350 nm and UV–Vis absorption spectrum (insert); **b** tandem mass spectrum obtained in positive ionization mode and proposed justification of fragment ions; **c** tandem mass spectrum obtained in negative ionization mode and proposed justification of fragment ions. The position of the charges on the molecular structures is only indicative.

Author contributions

MV and MW wrote the manuscript with contributions from all authors. MV, AOM, DT, MW, and SR carried out the non-invasive analysis. MV performed the invasive microanalysis. DT undertook the chromatographic analysis. MW served as the principal investigator for the project and provided overall supervision. All authors read and approved the final manuscript.

Availability of data and materials

The datasets used analyzed during the current study are available from the corresponding author on reasonable request.

Declarations

Competing interests

The authors declare that they have no competing interests.

Author details

[1]Northwestern University, Art Institute of Chicago Center for Scientific Studies in the Arts (NU-ACCESS), 2145 Sheridan Road, Evanston, IL 60208, USA. [2]Department of Scientific Research, The British Museum, Great Russell Street, London WC1B 3DG, UK. [3]Museo de Arte de Puerto Rico, 299 Avenida José

Vermeulen *et al. Heritage Science*   (2022) 10:44

Page 21 of 22

de Diego, Puerto Rico, San Juan 00909, USA. [4]Present Address: Centre for Art Technological Centre for Art Technological Studies and Conservation, Statens Museum for Kunst, Sølvgade 48-50, 1307 Copenhagen K, Denmark. [5]Present Address: M+, West Kowloon Cultural District, 38 Museum Drive, Kowloon, Hong Kong, China.

References

1. Sullivan EJ. From San Juan to Paris and back: Francisco Oller and Caribbean art in the era of impressionism. New Haven: Yale University Press; 2014.
2. Nuño JAGL. Pintura puertorriqueña durante il signlo XIX. Rev Inst Cult Puertorriq. 1979;84:22–35.
3. Mergal AM. Frade puertorriqueño pintor. Palique: Multi-Analytical Study of the Palette of Impressionist and Post-Impressionist Puerto Rican Artists; 1954.
4. Cottington D. Cubism in the shadow of war: the avant-garde and politics in Paris 1905–1914. New Haven: Yale University Press; 1998.
5. Antliff M. Inventing Bergson: cultural politics and the Parisian avant-garde. Princeton: Princeton University Press; 1993.
6. Roy A. The palettes of three impressionist paintings. Natl Gallery Tech Bull. 1985;9:12–20.
7. Roy A. Monet's palette in the twentieth century: 'Water-Lilies' and 'Irises.' Natl Gallery Tech Bull. 2007;28:58–68.
8. Pozzi F, van den Berg KJ, Fiedler I, Casadio F. A systematic analysis of red lake pigments in French Impressionist and Post-Impressionist paintings by surface-enhanced Raman spectroscopy (SERS). J Raman Spectrosc. 2014;45:1119–26. https://doi.org/10.1002/jrs.4483.
9. Pollack M. Odilon Redon, Paul Gauguin, and Primitivist Color. Art Bull. 2020;102:77–103. https://doi.org/10.1080/00043079.2020.1711488.
10. Thurrowgood D, Paterson D, de Jonge MD, Kirkham R, Thurrowgood S, Howard DL. A hidden portrait by Edgar Degas. Sci Rep. 2016;6:10. https://doi.org/10.1038/srep29594.
11. Hermens E, Wallert A. James McNeill Whistler: fluidity, finish and experiment. In: Proceedings of the Studying old master paintings: technology and practice. London: The National Gallery Technical Bulletin 30th Anniversary Conference; 2011. p. 229–36.
12. Mazzinghi A, Ruberto C, Castelli L, Ricciardi P, Czelusniak C, Giuntini L, Mandò PA, Manetti M, Palla L, Taccetti F. The importance of being little: MA-XRF on manuscripts on a Venetian island. X-Ray Spectrom. 2021;50:272–8. https://doi.org/10.1002/xrs.3181.
13. Delaney JK, Conover DM, Dooley KA, Glinsman L, Janssens K, Loew M. Integrated X-ray fluorescence and diffuse visible-to-near-infrared reflectance scanner for standoff elemental and molecular spectroscopic imaging of paints and works on paper. Herit Sci. 2018;6:31. https://doi.org/10.1186/s40494-018-0197-y.
14. Ricciardi P, Legrand S, Bertolotti G, Janssens K. Macro X-ray fluorescence (MA-XRF) scanning of illuminated manuscript fragments: potentialities and challenges. Microchem J. 2016;124:785–91. https://doi.org/10.1016/j.microc.2015.10.020.
15. Dal Fovo A, Mazzinghi A, Omarini S, Pampaloni E, Ruberto C, Striova J, Fontana R. Non-invasive mapping methods for pigments analysis of Roman mural paintings. J Cult Herit. 2020;43:311–8. https://doi.org/10.1016/j.culher.2019.12.002.
16. Delaney JK, Dooley KA, van Loon A, Vandivere A. Mapping the pigment distribution of Vermeer's Girl with a Pearl Earring. Herit Sci. 2020;8:4. https://doi.org/10.1186/s40494-019-0348-9.
17. Aceto M, Agostino A, Fenoglio G, Idone A, Gulmini M, Picollo M, Ricciardi P, Delaney JK. Characterisation of colourants on illuminated manuscripts by portable fibre optic UV-visible-NIR reflectance spectrophotometry. Anal Methods. 2014. https://doi.org/10.1039/c3ay41904e.
18. Baddini ALDQ, Santos JLVDP, Tavares RR, Paula LSD, Filho HDCA, Freitas RP. PLS-DA and data fusion of visible Reflectance, XRF and FTIR spectroscopy in the classification of mixed historical pigments. Spectrochim Acta Part A. 2022;265:120384. https://doi.org/10.1016/j.saa.2021.120384.
19. Delaney JK, Thoury M, Zeibel JG, Ricciardi P, Morales KM, Dooley KA. Visible and infrared imaging spectroscopy of paintings and
20. Glinsman L. The application of X-ray fluorescence spectrometry to the study of museum objects. Amsterdam: University of Amsterdam; 2004.
21. Pouyet E, Brummel K, Webster-Cook S, Delaney J, Dejoie C, Pastorelli G, Walton M. New insights into Pablo Picasso's La Miséreuse accroupie (Barcelona, 1902) using X-ray fluorescence imaging and reflectance spectroscopies combined with micro-analyses of samples. SN Appl Sci. 2020;2:1408. https://doi.org/10.1007/s42452-020-3130-4.
22. Vermeulen M, Tamburini D, Müller EMK, Centeno SA, Basso E, Leona M. Integrating liquid chromatography mass spectrometry into an analytical protocol for the identification of organic colorants in Japanese woodblock prints. Sci Rep. 2020;10:20921. https://doi.org/10.1038/s41598-020-77959-2.
23. Wainwright L. Americocentrism and Art of the Caribbean: Contours of a Time-Space Logic. J Am Stud. 2013;47:417–38. https://doi.org/10.1017/S0021875813000145.
24. Casey E. Visual culture of the Atlantic World. In: Heilbrunn timeline of art history. New York: The Metropolitan Museum of Art; 2018.
25. Hew D. Afro-Caribbean Art of Jamaica. In: Emancipation. Westport: Greenwood Publishing Group; 2001.
26. Cullen D, Fuentes Rodríguez E. Caribbean: art at the crossroads of the world. New York: El Museo del Barrio; 2012.
27. Kriz KD. Slavery, sugar, and the culture of refinement: picturing the British West Indies, 1700–1840. New Haven: Yale University Press; 2008.
28. Landau EG. Mexico and American modernism. New Haven: Yale University Press; 2013.
29. Flores T. Mexico's revolutionary avant-gardes: from Estridentismo to ¡30-30! New Haven: Yale University Press; 2013.
30. Duany J. Picturing Cuba: art, culture, and identity on the island and in the diaspora. Gainesville: University Press of Florida; 2019.
31. Heuman G. Victorian Jamaica. Durham: Duke University Press; 2018.
32. Pouyet E, Barbi N, Chopp H, Healy O, Katsaggelos A, Moak S, Mott R, Vermeulen M, Walton M. Development of a highly mobile and versatile large MA-XRF scanner for in situ analyses of painted work of arts. X Ray Spectrom. 2020. https://doi.org/10.1002/xrs.3173.
33. Solé VA, Papillon E, Cotte M, Walter P, Susini J. A multiplatform code for the analysis of energy-dispersive X-ray fluorescence spectra. Spectrochim Acta Part B. 2007;62:63–8. https://doi.org/10.1016/j.sab.2006.12.002.
34. Schindelin J, Arganda-Carreras I, Frise E, Kaynig V, Longair M, Pietzsch T, Preibisch S, Rueden C, Saalfeld S, Schmid B, et al. Fiji: an open-source platform for biological-image analysis. Nat Methods. 2012;9:676–82. https://doi.org/10.1038/nmeth.2019.
35. Preibisch S, Saalfeld S, Tomancak P. Globally optimal stitching of tiled 3D microscopic image acquisitions. Bioinformatics. 2009;25:1463–5. https://doi.org/10.1093/bioinformatics/btp184.
36. Vermeulen M, Smith K, Eremin K, Rayner G, Walton M. Application of Uniform Manifold Approximation and Projection (UMAP) in spectral imaging of artworks. Spectrochim Acta Part A Mol Biomol Spectrosc. 2021;252:119547. https://doi.org/10.1016/j.saa.2021.119547.
37. Vermeulen M, Müller EMK, Leona M. Non-invasive study of the evolution of pigments and colourants use in 19th century Ukiyo-e. Hong Kong: Arts of Asia; 2020. p. 50.
38. Ivdsc FR. Fiber optics reflectance spectra (FORS) of pictorial materials in the 270–1700 nm range. Florence: Institute for Applied Physics "Nello Carrara" of the National Research Council; 2020.
39. Burgio L, Clark RJH. Library of FT-Raman spectra of pigments, minerals, pigment media and varnishes, and supplement to existing library of Raman spectra of pigments with visible excitation. Spectrochim Acta Part A Mol Biomol Spectrosc. 2001;57:1491–521. https://doi.org/10.1016/s1386-1425(00)00495-9.
40. Coccato A, Bersani D, Coudray A, Sanyova J, Moens L, Vandenabeele P. Raman spectroscopy of green minerals and reaction products with an application in Cultural Heritage research. J Raman Spectrosc. 2016;47:1429–43. https://doi.org/10.1002/jrs.4956.
41. Saverwyns S. Russian avant-garde… or not? A micro-Raman spectroscopy study of six paintings attributed to Liubov Popova. J Raman Spectrosc. 2010;41:1525–32. https://doi.org/10.1002/jrs.2654.
42. Fremout W, Saverwyns S. Identification of synthetic organic pigments: the role of a comprehensive digital Raman spectral library. J Raman Spectrosc. 2012;43:1536–44. https://doi.org/10.1002/jrs.4054.

Vermeulen *et al. Heritage Science*   (2022) 10:44

Page 22 of 22

43. Scherrer NC, Stefan Z, Francoise D, Annette F, Renate K. Synthetic organic pigments of the 20th and 21st century relevant to artist's paints: Raman spectra reference collection. Spectrochim Acta Part A Mol Biomol Spectrosc. 2009;73:505–24. https://doi.org/10.1016/j.saa.2008.11.029.

44. Ganz JA, Groom G, Ireson N, Jaros D, Muir K, Nichols K, Shaw J. Monet paintings and drawings at the Art Institute of Chicago. Chicago: The Art Institute of Chicago; 2014.

45. Walter P, Sarrazin P, Gailhanou M, Hérouard D, Verney A, Blake D. Full-field XRF instrument for cultural heritage: application to the study of a Caillebotte painting. X Ray Spectrom. 2019;48:274–81. https://doi.org/10.1002/xrs.2841.

46. Schaefer I, Lewerentz K, Saint-George CV. Painting light: the hidden techniques of the Impressionists. Milano: Skira; 2008. p. 238.

47. Burnstock A, Gutiérrez L. Technical examination of works by Camille and Lucien Pissarro from the Courtauld Gallery. Pennsylvania: Art Matters Studio; 2013.

48. Centeno SA, Hale C, Carò F, Cesaratto A, Shibayama N, Delaney J, Dooley K, van der Snickt G, Janssens K, Stein SAV. Gogh's Irises and Roses: the contribution of chemical analyses and imaging to the assessment of color changes in the red lake pigments. Heritage Science. 2017;5:18. https://doi.org/10.1186/s40494-017-0131-8.

49. Monico L, Janssens K, Miliani C, Brunetti BG, Vagnini M, Vanmeert F, Falkenberg G, Abakumov A, Lu Y, Tian H, et al. Degradation process of lead chromate in paintings by Vincent van Gogh studied by means of spectromicroscopic methods. 3. Synthesis, characterization, and detection of different crystal forms of the chrome yellow pigment. Anal Chem. 2013;85:851–9. https://doi.org/10.1021/ac302158b.

50. Lizun D, Kurkiewicz T, Szczupak B. Exploring Liu Kang's Paris Practice (1929–1932): insight into painting materials and technique. Heritage. 2021;4:828–63.

51. CAMEO. The Conservation and Art Materials Encyclopedia Online (CAMEO). http://cameo.mfa.org/wiki/Tartrazine. Accessed 1 Oct 2022.

52. Kleiner S, Pouyet E, Oakley L. Tissot's painting technique. In: Buron ME, editor. James Tissot. San Francisco: PRESTEL; 2019. p. 238–45.

53. Singer B, Aslaksby TE, Topalova-Casadiego B, Tveit ES. Investigation of materials used by Edvard Munch. Stud Conserv. 2010;55:274–92.

54. American Association of Textile Chemists and Colorists. Colour index. 3rd ed. Bradford: The Society of Dyers and Colourists; 1971.

55. MacEvoy, B. Handprint. https://www.handprint.com/HP/WCL/watery.html. Accessed 1 Oct 2022.

56. De Keijzer M. The history of modern synthetic inorganic and organic artists' pigments. London: James & James; 2002. p. 42.

57. News PRA. Francisco Oller y sus tradicionales bodegones autóctonos. San Juan: La Editorial, UPR; 2021.

Publisher's Note